CHAPTER TEN

In Vivo Measurements of Blood Flow and Glial Cell Function with Two-Photon Laser-Scanning Microscopy

Fritjof Helmchen* *and* David Kleinfeld†

Contents

Abstract

Two-photon laser scanning microscopy is an ideal tool for high-resolution fluorescence imaging in intact organs of living animals. With regard to *in vivo* brain research, this technique provides new opportunities to study hemodynamics in the microvascular system and morphological dynamics and calcium signaling in various glial cell types. These studies benefit from the ongoing developments for *in vivo* labeling, imaging, and photostimulation. Here, we review recent advances in the application of two-photon microscopy for the study of blood flow and glial cell function in the neocortex. We emphasize the dual role of two-photon imaging as a means to assess function in the normal state as well as a tool to investigate the vascular system and glia under pathological conditions,

* Department of Neurophysiology, Brain Research Institute, University of Zurich, Zurich, Switzerland
† Department of Physics, University of California, San Diego, La Jolla, California

Methods in Enzymology, Volume 444
ISSN 0076-6879, DOI: 10.1016/S0076-6879(08)02810-3

such as ischemia and microvascular disease. Further, we show how extensions of ultra-fast laser techniques lead to new models of stroke, where individual vessels may be targeted for occlusion with micrometer precision.

1. Introduction

All tissues are mixtures of various cellular components that perform specialized tasks. In the central nervous system (CNS), several cellular structures exist along with the electrically excitable neuronal cells that process information and fulfill the primary job of the CNS. All neuronal networks within the brain are tightly interwoven with networks of glial cells, and thus the underlying microvasculature. The three major subtypes of glial cells are astrocytes, oligodendrocytes, and microglial cells (Fig. 10.1).

Astrocytes have long been recognized for their predominant role in maintaining the homeostasis of neurons. They contribute to the regulation of local blood supply and provide nutrition to the neurons. More recently it has been recognized that the communication between astrocytes and neurons is much tighter than previously thought, for example via the release of gliotransmitters from astrocytes and through the ability of astrocytes to sense glutamate

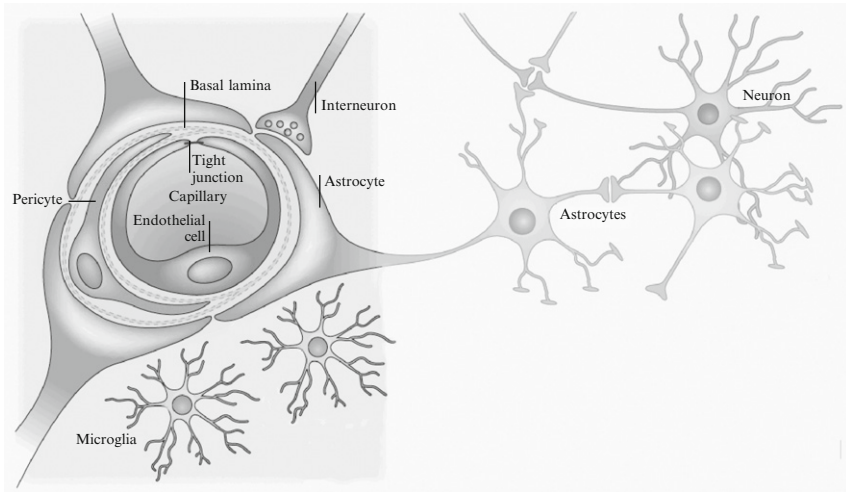

Figure 10.1 Vascular constituents of the rodent blood–brain barrier. The barrier is formed by capillary endothelial cells that form the capillary wall. These are surrounded by basal lamina, pericytes, and astrocytic perivascular endfeet. Astrocytes provide one cellular link to neurons; the other is supplied by direct connections from inhibitory interneurons. The figure also shows microglial cells that populate the brain. (Adapted from Abbott, N. J., Rönnbäck, L., and Hansson, E. (2006). Astrocyte–endothelial interactions at the blood–brain barrier. *Nat. Rev. Neurosci.* **7**, 41–53.)

(Volterra and Meldolesi, 2005). Astrocytes are also closely linked to the microvasculature system. Their "endfeet" enwrap the entire vasculature system so that they are in continuous communication with the endothelial cells. In the brain, endothelial cells from a tight blood–brain barrier, which leads to immunological isolation of the brain. Recent work has probed the *in vivo* dynamics of astroglial signaling in the control of blood flow (Takano *et al.*, 2006) and following sensory stimulation (Wang *et al.*, 2006). Lastly, recent evidence suggests that astrocytes have important physiological functions on the scale of individual synapses as well as on the level of neural circuits.

Oligodendrocytes are the myelin-producing cells of the CNS and play a role roughly analogous to Schwann cells in the peripheral nervous system. Oligodendroctytes form the myelin sheets around a neuronal axon, particularly in the long-range axonal tracts that form the white matter, and accelerate the propagation of action potentials. Finally, microglial cells are the immune-competent cells in the CNS. In contrast to astrocytes and oligodendrocytes, which are of ectodermal origin, microglial cells derive from the mesoderm and are part of the mononuclear phagocytic system. Microglial cells invade the brain during development and become permanent residents. They can be activated by a variety of stimuli, mostly in response to any kind of tissue injury, and quickly transform into phagocyting cells. Recent work, detailed below, has probed the *in vivo* dynamics of microglia during resting conditions and in response to brain vascular injury (Davalos *et al.*, 2005; Nimmerjahn *et al.*, 2005).

We now turn to the angioarchitecture of the vascular system *per se*. The topology of arteriole networks varies among different brain regions. In the neocortex, the topology is stereotyped and well understood (Fig. 10.2). The surface of cortex is covered by highly interconnected mesh-like networks of arterioles formed by anastomoses between branches of the great cerebral arteries (Brozici *et al.*, 2003). The most studied of these is the network formed by anastomoses of the middle cerebral artery, which supplies parietal cortex and parts of the striatum. Recent data support the notion that the surface network functions as an ideal grid, so that interruption to flow at a single point receives compensation from flow in neighboring regions (Schaffer *et al.*, 2006). The subsurface microvascular also forms a series of loops, in three rather than two dimensions. While these loops are quite tortuous, their detailed organization is a topic of ongoing research. Finally, the penetrating arterioles connect the surface arteriole network to the underlying microvessels that course throughout the parenchyma. The penetrating arterioles are bottlenecks, in that occlusion of a single penetrating vessel leads to a loss of supply to all microvessels in the territory fed by that arteriole (Nishimura *et al.*, 2007). Recent work, detailed below, considers the changes in blood flow dynamics that accompany a single, targeted occlusion (Nishimura *et al.*, 2006; Schaffer *et al.*, 2006) as a model of microstroke (Vermeer *et al.*, 2003).

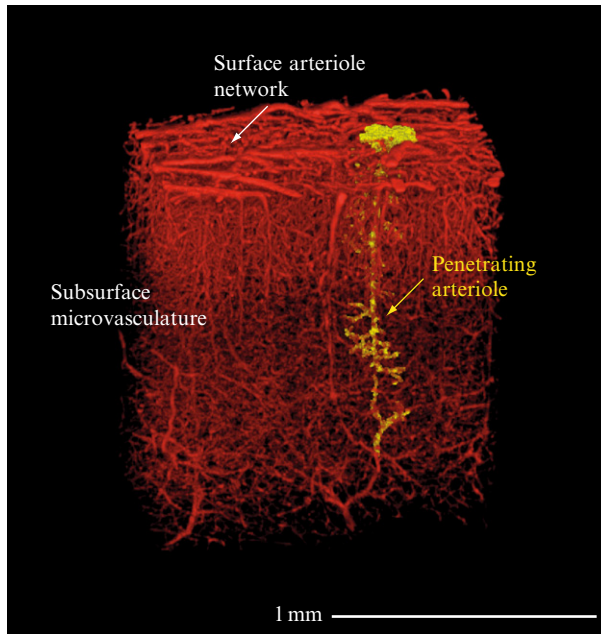

Figure 10.2 Major vascular topologies in the supply of blood to neocortex. The vasculature of a mouse was filled with fluorescently labeled agarose and a region imaged with the all-optical histology method (see Tsai *et al.*, 2005). The reconstructed image was highlighted in the vicinity of a single penetrating arteriole (yellow hue). (From unpublished data of P. S. Tsai and P. Blinder in the Kleinfeld laboratory.)

2. Two-Photon Microscopy of Fluorescent Labels as a Tool for Brain Imaging

Historically, experimental methods to investigate glial function in the intact brain have been limited. Different from neurons, glial cells are electrically mostly silent, which makes them invisible to standard *in vivo* electrophysiological methods, such as extracellular recordings. Similarly, a fine-scale investigation of blood flow down to the level of individual capillaries has been difficult, although coarse measurements of spatially averaged blood flow in the brain are routinely performed, such as by laser Doppler flowmetry. Advances in imaging technologies that have been achieved during the past decade now provide a means to investigate blood flow and glial function *in vivo*. The key technology is two-photon laser-scanning fluorescence microscopy (TPLSM) (Denk *et al.*, 1990, 1994), which can achieve penetration depths of 500 to 1000 μm into tissue (Helmchen and Denk, 2005). Two-photon microscopy not only provides micrometer spatial resolution deep within the tissue, but also permits

dynamic measurements over a wide range of time scales, ranging from milliseconds to years. Besides improvements in microscope technology (Helmchen and Denk, 2002), the development of various techniques for fluorescence labeling of specific tissue components *in vivo* has been of utmost importance. In particular, many variants of fluorescent proteins (FPs) have been created as anatomical markers or biosensors. These constructs can be specifically expressed in particular subsets of cells and are revolutionizing the field of neuroscience by opening new possibilities to study cellular dynamics in the living animal (Garaschuk *et al.*, 2007; Kleinfeld and Griesbeck, 2005; Miyawaki, 2005). In the following discussion, we restrict our focus to progress that has been made for *in vivo* labeling of the components of the vascular and the glial system in mice and rats. We highlight emerging applications for revealing their functions under both physiological and pathological conditions.

2.1. Animal preparation

Most measurements of blood flow dynamics and glial function involve acute experiments with anesthetized animals. Access to the cortex is through a craniotomy (Kleinfeld and Delaney, 1996), although with transgenic mice a thinned-skull preparation may be used with the advantage that the dura may be kept intact (Frostig *et al.*, 1993; Grutzendler *et al.*, 2002). A metal frame (Fig. 10.3A) is employed both as part of a chamber above the craniotomy, or thinned skull, and as a support for the animals head in the imaging apparatus (Fig. 10.3B). We typically mount the animal and all support gear, including air/gas supplies, on a single plate in our surgical suite and then move the entire plate to the microscope (Kleinfeld *et al.*, 2008) (Fig. 10. 3C). Anesthesia, airway condition, and body temperature are maintained throughout the experiment and blood gases can be collected, typically every 4 h with rats, to assess the health of the animals.

2.2. *In vivo* staining of blood vessels and glial cells

Labeling of the structures of interest with appropriate fluorescent markers is a prerequisite for dissecting cellular functions with the use of TPLSM. Such markers label cells or cellular structures as a means to identify cells and target them for experimental manipulations. Further, markers may also have a functional dependence, such that their fluorescence properties change according to changes in particular physiological parameters, such as intracellular calcium concentration. We focus on methods that are available for staining components of the vascular and glial system in the rodent brain; reviews of methods for *in vivo* staining of neurons and neuronal networks can be found elsewhere (Feng *et al.*, 2000; Garaschuk *et al.*, 2006b, 2007; Göbel and Helmchen, 2007).

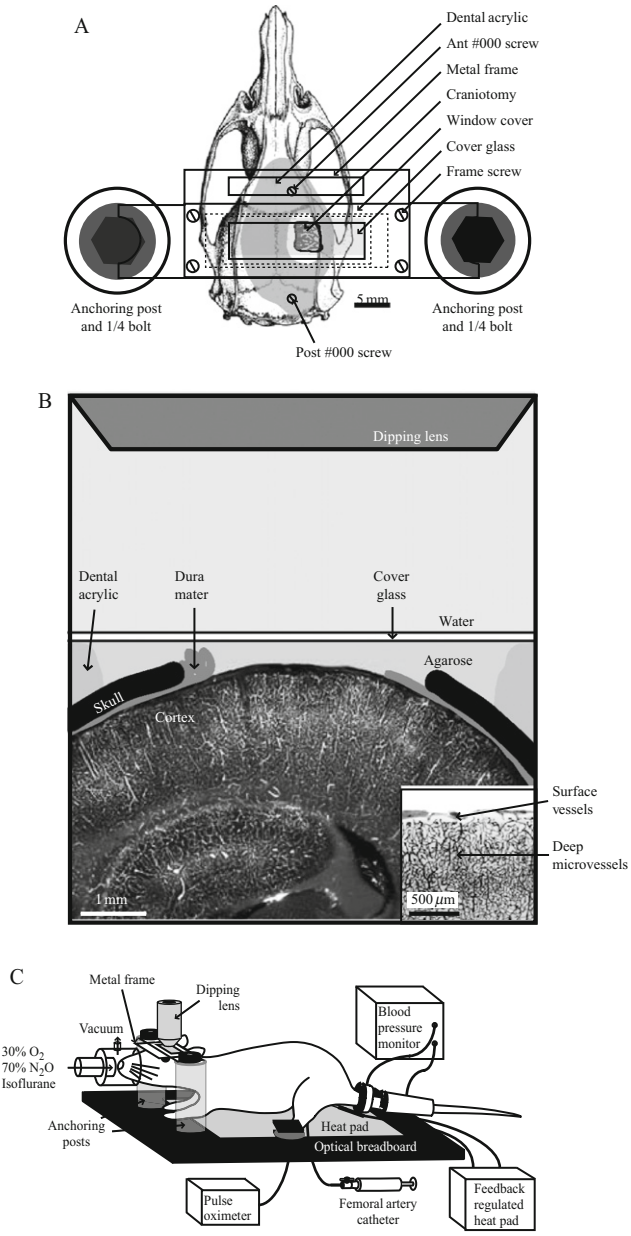

Figure 10.3 Method for *in vivo* imaging through a cranial window. (A) A metal frame with a glass window over the craniotomy immobilizes the head of the animal during imaging. (B) A cross-sectional view of the cranial window. The inset diagram shows an inverted coronal view of surface vessels and deep microvessels that are targeted for occlusion. (C) The metal frame attached to the skull is immobilized between two anchoring posts inserted into an optical breadboard. Anesthesia is maintained

2.2.1. Blood plasma

The blood vessel system can be easily labeled by injection of a bolus of fluorescent dye into the blood stream through either a tail vein or a femoral artery catheter. This approach requires the use of high-molecular-weight carrier molecules, typically 2 MDa dextran, to minimize the excretion of the dye. Such labeling stains only the blood plasma and is ideal for automated particle tracking since flowing red blood cells (RBCs) appear as shadows against a bright background (Fig. 10.4) (Kleinfeld *et al.*, 1998). Either fluorescein- or rhodamine-derivatized dextrans are injected as green or red markers, respectively. Various parameters of microcirculation, including the topological organization of local blood flow and the density, flux, and speed of RBCs, may be quantified. Alternately, RBCs may be labeled directly through the use of a donor animal (Sarelius and Duling, 1982). In this case, a fraction of the RBCs are bright, which is advantageous for calculating speeds in vessels with relatively high velocity as the process of particle tracking is considerably simplified.

Staining of the blood plasma has utility beyond the ability to track RBCs. From an anatomical perspective, high-contrast staining of the microvasculature provides clear landmarks for repeatedly finding the same field of view in long-term imaging studies (Bacskai *et al.*, 2001, 2002). Further, fluorescent staining can help to target experimental manipulations, such as photodisruption or photoinduction of thrombosis, to specific vessels and to verify and visualize subsequent extravasation.

2.2.2. Glial cells

Several methods are available for fluorescence staining of glial cells *in vivo*, including the expression of FPs, discussed below, and the application of synthetic organic dyes. Astrocytes in the neocortex of rats and mice can be readily stained by sulforhodamine 101 (SR101), a water-soluble red fluorescent dye. Brief topical application of SR101 to the exposed surface of the intact neocortex results in bright staining of the astrocyte network (Nimmerjahn *et al.*, 2004). The specificity of the stain for astrocytes verified in three ways: (a) postmortem immunohistochemistry with antibodies against common markers of neurons and glial subtypes indicates that the SR101-labeled cells co-labeled as astrocytes; (2) application of SR101 to transgenic

with a gas mixture. Blood pressure is measured with a tail-cuff device. The femoral artery catheter is used to collect blood samples for blood gas measurements, and is also the delivery route for contrast agents that stain the blood plasma. Heart rate and blood oxygen saturation are continuously monitored using a pulse oximeter. (Adapted from Kleinfeld, D., Friedman, B., Lyden, P. D., and Shih, A. Y. (2008). Targeted occlusion to surface and deep vessels in neocortex via linear and nonlinear optical absorption. In: Chen, J., Xu, X.-M., Zhang, J., eds. "Animal Models of Acute Neurological Injuries." Humana Press, Inc., Totowa, pp. 19–185)

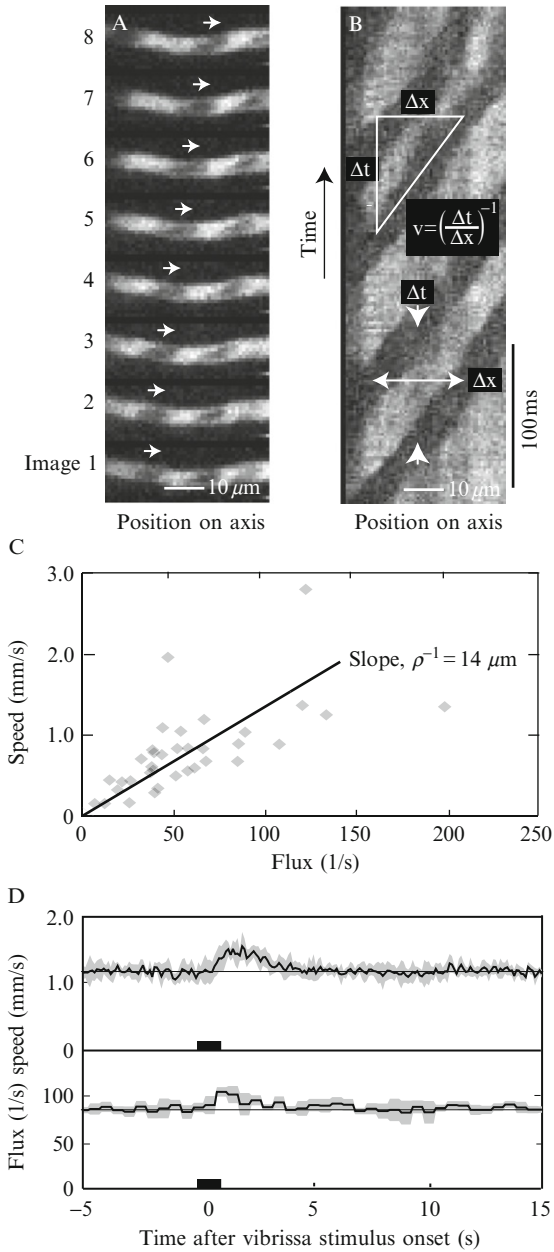

Figure 10.4 Imaging of capillary blood flow in cortex with fluorescently labeled plasma. (A) Successive planar images through a capillary, at a depth of 450 μm below the pial surface, acquired every 60 ms. The change in position of a particular unstained object, interpreted as a RBC, is indicated by the series of arrows (→); the velocity of the RBC is +0.18 mm/s. (B) Characterization of the transport of RBCs in capillaries.

animals with astrocyte-specific expression of enhanced green fluorescent protein (EGFP) results in a complete overlap of exogenous and endogenous markers; and (3) counterstaining the blood plasma with fluorescein/dextran reveals that the entire vasculature system is sheathed by astrocytic endfeet (Fig. 10. 5A). The mechanism of SR101 uptake remains, however, unclear. SR101 can be transported by multi–drug-resistant proteins, but this transport mechanism usually extrudes SR101 from the cytosol. Perhaps astrocytes possess similar transporter proteins that operate in reverse mode, shuffling SR101 inside the cell. Once inside cells, SR101 easily distributes throughout the astrocyte network. Evidence suggests that the distribution is via gap junctions (Nimmerjahn *et al.*, 2004).

There appears to be confusion in the literature with regard to the specificity of glial SR101 uptake in brain slices and in brain regions aside from neocortex. Early studies reported that SR101 stains oligodendroglia in the retina (Ehinger *et al.*, 1994) and labels activated neurons in a turtle brainstem–cerebellum preparation (Keifer *et al.*, 1992). A difficulty with brain slices is that SR101 is apparently taken up by dead or damaged cells near the tissue surface. Further, as shown in a recent report that demonstrated SR101 labeling of astrocytes in hippocampal slices (Kafitz *et al.*, 2008), efficient SR101 uptake requires physiological temperature. An additional issue is that the mode of SR101 application may matter. In the cerebellum, it was originally reported that SR101 fails to stain Bergmann glia (Nimmerjahn *et al.*, 2004). However, in recent experiments bright SR101-staining of Bergmann glia was achieved by directly injecting the dye through a micropipette into the tissue, rather than applying it topically to the surface (unpublished data of W. Göbel in the Helmchen laboratory). Hence, specific properties of ependymal cells and their connections to the parenchymal glial network may be important for dye uptake from the tissue surface. *In toto*, SR101 is a simple and robust stain of astrocytes in the rodent neocortex *in vivo*, but further work is required to fully understand regional differences in staining and the uptake mechanism of the dye.

The vessel was longitudinally scanned in line scan mode at 2 ms/line. The instantaneous velocity is $v_{cap} = \Delta x/\Delta t$; the flux, F_{cap}, is $1/\triangle t$, and the linear density is $\rho_{cap} = 1/\Delta x$. (C) Plot of the speed versus flux. The solid line is a best fit and corresponds to the density (Eq. 10.1). (D) The trial-averaged response of RBC flow to vibrissa stimulation. We recorded from a single capillary in vibrissa S1 cortex at a depth of 255 μm below the dura. The dark line is the average over all six trials, the gray band is the standard deviation of the average. Black bar indicates the whisker stimulation period. (Adapted from Kleinfeld, D., Mitra, P. P., Helmchen, F., and Denk, W. (1998). Fluctuations and stimulus-induced changes in blood flow observed in individual capillaries in layers 2 through 4 of rat neocortex. *Proc. Natl. Acad. Sci. U.S.A.* 95, 15741–15746.)

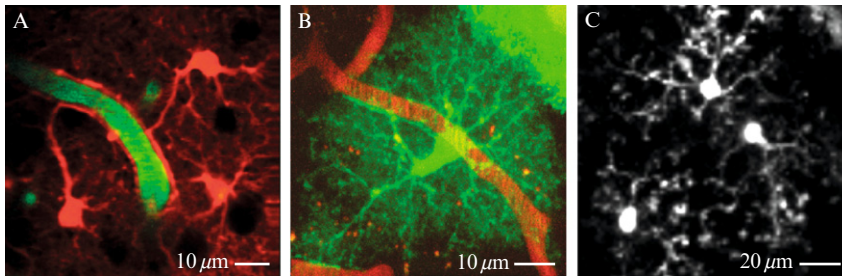

Figure 10.5 Examples of *in vivo* fluorescence staining of vasculature and glial cells. (A) Co-staining of microvessels and astrocytes by injection of fluorescein/dextran into the blood plasma and topic application of SR101 to the brain surface. (B) An EGFP-expressing astrocyte in an hGFAP/EGFP transgenic mouse. The enwrapped blood capillary was visualized by tail-vein injection of rhodamine/dextran. (C) *In vivo* TPLSM image of three EGFP-expressing microglial cells in the neocortex of CX3CR1/EGFP mice. (Images in (A) and (C) are adapted, respectively, from Nimmerjahn, A., Kirchhoff, F., Kerr, J. N., and Helmchen, F. (2004). Sulforhodamine 101 as a specific marker of astroglia in the neocortex *in vivo*. *Nat. Methods* **29,** 31–37; and Nimmerjahn, A., Kirchhoff, F., and Helmchen, F. (2005). Resting microglial cells are highly dynamic surveillants of brain parenchyma *in vivo*. *Science* **308,** 1314–1318.)

2.2.3. Expression of fluorescent proteins

The alternate approach for specific *in vivo* staining of glial cells is the expression of FPs. While local transfection with viral constructs using an unspecific promoter such as the ubiquitin promoter can result in staining of some glial cells, this labeling is sparse and uncontrolled. Better results are obtained by generation of transgenic animals through the use of specific promoters. Meanwhile, there are a number of transgenic mouse lines with specific glial expression pattern available. For example, astrocytes can be visualized in transgenic mouse lines that express FPs under control of the promoter for human–glial-fibrillary-acid protein (GFAP), which is glia-specific (Zhuo *et al.*, 1997; Nolte *et al.*, 2001) (Fig. 10.5B). Other transgenic mouse lines show FP expression in non-astrocytic glial cells, including oligodendrocytes (Fuss *et al.*, 2000) and microglial cells (Jung *et al.*, 2000). In the latter case a knock-in approach was used to introduce the gene sequence for EGFP into the gene locus of the fractalkine receptor (CX3CR1). The chemokine fractalkine is a transmembrane glycoprotein that is found in endothelial cells and neurons and can be released in a soluble form following proteolytic cleavage (Cook *et al.*, 2001). In the CNS, microglial cells are the only cells that express CX3CR1. As a result, they are selectively labeled with high contrast with respect to background fluorescence (Fig. 10.5C), which make them very well suited for *in vivo* imaging studies.

2.3. Functional imaging

2.3.1. Blood flow

Blood flow can be most readily measured in capillaries, where the RBCs pass in single file. A line-scan through a capillary leads to a sequence of bright pixels, corresponding to labeled plasma, and dark pixels, corresponding to RBCs (Fig. 10.4A). This results in diagonal bands in a space–time image constructed from the line-scan data (Fig. 10.4B). The slope of the bands is the inverse of the velocity, denoted v_{cap}, which may be determined automatically. The linear flux is found by counting the number of RBCs that pass per unit time. The flux, F_{cap}, and velocity are related by

$$F_{cap} = \rho v_{cap} \tag{10.1}$$

A plot of v_{cap} versus F_{cap} shows a fairly linear relation (Fig. 10.4C), which implies that the linear density, ρ, and thus the hematocrit, is constant. As an application, we consider possible changes in the speed and flux concurrent with sensory stimulation. An example measurement from the vibrissa primary sensory cortex shows that the speed and flux of RBCs in a single capillary both increase concomitant with brief motion of the vibrissae (Kleinfeld *et al.*, 1998) (Fig. 10.4D).

A more interesting case of blood flow dynamics concerns flow in large vessels. The line-scan scheme can be used to measure flow so long as the flow is laminar, that is, the speed along a line parallel to the vessel stays constant (Fig. 10.6A and B). This can be shown self-consistently by measuring the velocity at different radii from the centerline and plotting the speed as a function of the radius (Fig. 10.6C). We expect to get Poiseuille's parabolic curve, that is,

$$v(r) = \frac{\Delta P}{4L\eta}\left(R^2 - r^2\right) \tag{10.2}$$

slightly flattened by the non-zero size of the RBC, where ΔP is the pressure drop across a vessel of length L and radius R and η is effective viscosity. In practice, this condition is fulfilled (Fig. 10.6C). This implies that the blood flows as a series of nested cylinders, fastest in the center and slower toward the walls. The average velocity across the cross-section of the vessel is $\langle v \rangle = (\Delta P/8\eta L)R^2$, so that $\langle v \rangle = v(0)/2$ where $v(0)$ is the measured center-line velocity. The volume flux is

$$F_{vol} = \langle v \rangle A = \frac{\Pi}{2} v(0) R^2 \tag{10.3}$$

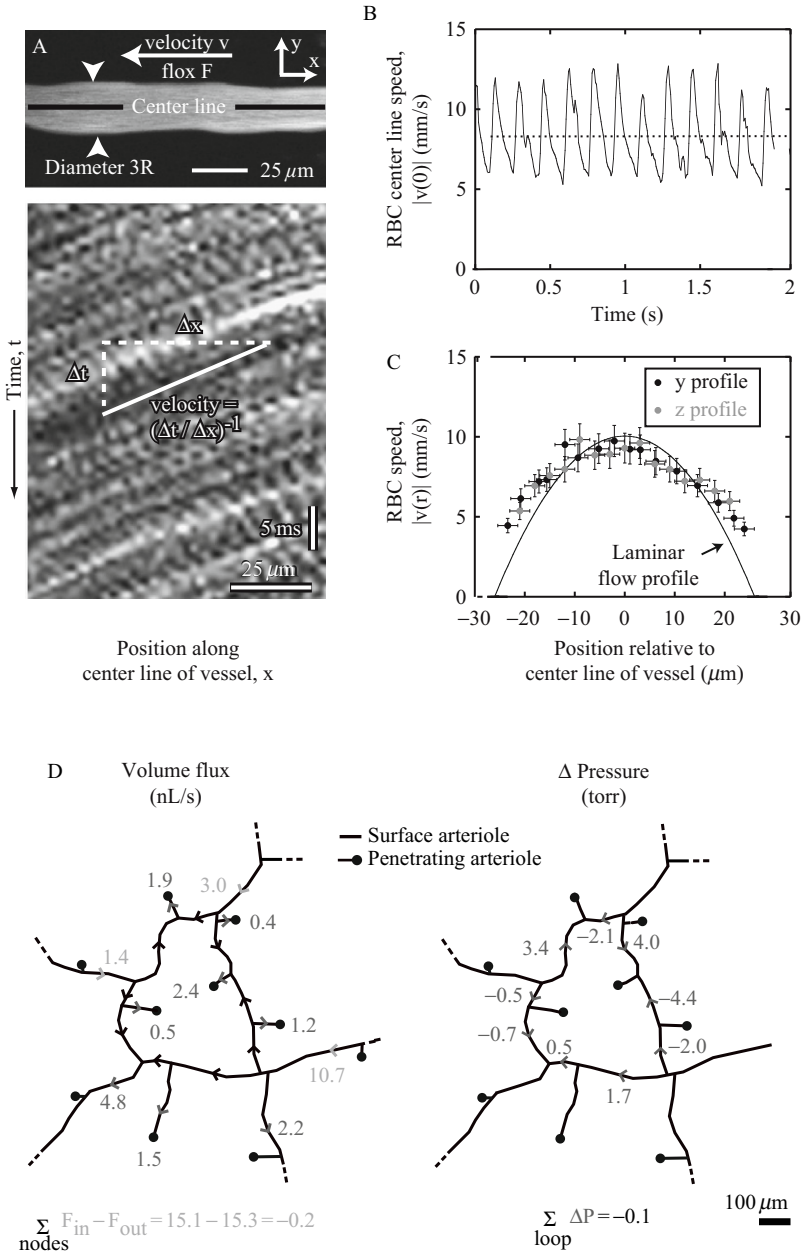

Figure 10.6 Imaging of blood flow in pial arterioles with fluorescently labeled plasma. (A, top) Maximum-intensity projection of a TPLSM image stack through a cortical arteriole. The dark line indicates the location where the line-scan data was taken, and the arrow represents the direction of flow obtained from these scans. (A, bottom) Line-scan data from the vessel in top panel forms a space-time image with time running down the image. The dark streaks running from upper right to lower left are formed by the motion of the

Lastly, the pressure versus velocity relation can be written in the form of Ohm's law, with ΔP playing the role of potential drop, $\langle v \rangle$ playing the role of current, and $8\Pi\eta$ playing the role of resistivity, that is,

$$\Delta P = F_{vol}\frac{8\eta L}{\pi R^4} = \left(8\pi\eta\frac{L}{\pi R^2}\right)\langle v\rangle \qquad (10.4)$$

Plots of the flux into and out of a region of the brain are useful as a means to study RBC utilization. They also act as a methodological control, as the flux into a loop must equal the flux out of that loop. This is illustrated in Fig. 10.6D, for which the total flux balances to within 2%. A similar zero-sum rule holds for the pressure drops along a vascular loop (Fig. 10.6D); here we see that the total pressure drop sums to within 5% of the average drop across a given segment.

2.3.2. Astrocyte dynamics

Beyond issues of determining network structure and cell morphology, fluorescence imaging is a powerful tool for assessing the functional state of cells. The most common functional markers are fluorescent indicators of intracellular calcium, which can be loaded into neuronal and glial cell populations in the neocortex *in vivo*. The simplest method for loading is to apply the membrane-permeable acetoxymethyl(AM)-ester form of indicator, which is nonspecifically taken up and trapped inside cells once the ester groups have been cleaved by endogenous esterases. For unknown reason some indicators, such as Fluo-4/AM and Rhod-2/AM, are preferentially taken up by astrocytes, at least when topically applied to the brain surface (Hirase *et al.*, 2004; Takano *et al.*, 2006). In contrast, Oregon-Green BAPTA-1/AM (OGB-1) labels both the neuronal and glial networks

nonfluorescent RBCs. The RBC speed is given by the inverse of the slope of these streaks, while the direction of flow is discerned from the sign of the slope. (B) RBC speed along the center of the arteriole shown in part (A) as a function of time. The periodic modulation of the RBC speed occurs at the ~6-Hz heart rate. The dotted line represents the temporal average of the speed. (C) RBC speed in a different, larger arteriole, averaged over 40 s, as a function of the transverse position in the vessel along horizontal (y) and vertical (z) directions. The parabolic curve (Eq. 10.2) represents the laminar flow profile that most closely matches the data, that is, $v(r) = (A/R^2) - (R^2 - r^2)$, where v is the velocity of the RBCs, R is the measured vessel radius of 26 μm, and A is a free parameter (A = 10 mm/s). (D) Example data from measurements around a closed loop of pial vessels and the vessels that flow into and out of the loop. We measured the radius and length, L, of each segment, along with the centerline velocity, v(0). The volume flux was calculated according to Eq. 10.3, and the pressure drops were calculated according to Eq. 10.4 with $\eta = 5 \times 10^{-3}$ Pa • s (1 Torr ~ 133 Pa). Ideally, the total flux should be zero and the total pressure drop should be zero; the actual values differ slightly. (Panels (A) to (C) are adapted from Schaffer, C. B., Friedman, B., Nishimura, N., Schroeder, L. F., Tsai, P. S., Ebner, F. F., Lyden, P. D., and Kleinfeld, D. (2006). Two-photon imaging of cortical surface microvessels reveals a robust redistribution in blood flow after vascular occlusion. *Public Library Sci. Biol.* 4, 258–270.)

(Garaschuk *et al.*, 2006a; Stosiek *et al.*, 2003). The green fluorescence of OGB-1 permits counterstaining with red fluorescent SR101 (Nimmerjahn *et al.*, 2004) to yield a crisp discrimination of astrocytic versus neuronal networks (Fig. 10.7A). It is unclear whether microglial cells load calcium indicators because they remain invisible within the diffusely stained background.

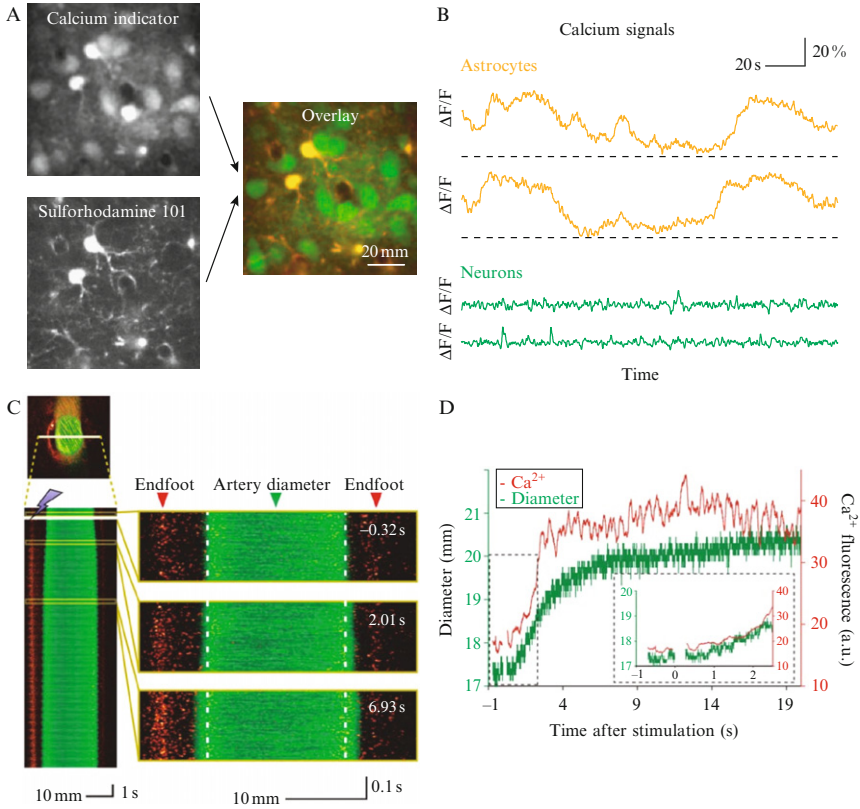

Figure 10.7 *In vivo* measurement of astrocyte function performed with TPLSM. (A) Multicell bolus loading of the calcium indicator OGB-1 into cortical layer 2 stains astrocytes as well as neurons. The astrocyte-specific SR101 stain unambiguously labels only astrocytes. (B) Spontaneous slow intracellular calcium oscillations occur in astrocyte cell bodies. Brief neuronal calcium transients, presumably coupled to action-potential firing, occur in neurons. (C) Images of a vascular astrocyte loaded with the Ca^{2+} indicator dye Rhod-2/AM (red) and DMNP-EDTA/AM, a caged Ca^{2+} compound. Light-induced Ca^{2+} uncaging in the astrocytic endfoot triggered vasodilation. Vasculature was stained with fluorescein/dextran (green). Purple arrow indicates the position of photostimulation. Scale bar, 10 μm. (D) Time course of astrocytic Ca^{2+} increase (red) and arterial vasodilation (green) following photostimulation. (Panel (B) is adapted from Takano, T., Tian, G. F., Peng, W., Lou, N., Libionka, W., Han, X., and Nedergaard, M. (2006). Astrocyte-mediated control of cerebral blood flow. *Nat. Neurosci.* **9**, 260–267.)

Several laboratories have started to investigate astroglial calcium signaling *in vivo*. In anesthetized animals, neocortical astrocytes show spontaneous calcium oscillations and waves (Fig. 10.7B) (Hirase *et al.*, 2004; Nimmerjahn *et al.*, 2004). A caveat is that the rate of these spontaneous events increases with laser illumination power (Wang *et al.*, 2006) so that laser power should be kept as low as possible to avoid artifacts. Astrocytes also communicate with various other tissue components. For example, their endfeet are in tight contact with endothelial cells, enabling astrocytes to participate in regulation of local blood flow. Using a combination of *in vivo* TPLSM and uncaging of caged Ca^{2+}, Takano *et al.* (2006) demonstrated that intracellular calcium elevation in glial endfeet alone could cause a rapid and transient dilation of the associated vessel (Fig. 10.7C and D).

A close functional relationship of astroglia with the surrounding neuronal network is indicated by the recent finding of sensory-evoked calcium signals in astrocytes (Wang *et al.*, 2006). These signals were inhibited by antagonists of metabotropic, but not ionotropic, glutamate receptors. This suggests a direct action of synaptically released glutamate on astrocytes. The functional implications of this finding remain to be elucidated, in particular for cortical processing in awake animals. Finally, *in vivo* imaging of astroglia calcium signaling provides new promising means to investigate functional alterations under various conditions of brain pathology, such as epilepsy (Tian *et al.*, 2005) and neurodegenerative diseases (Eichhoff *et al.*, 2008).

2.3.3. Microglia dynamics

Microglial cells are the primary immune effector cells in the CNS and they are known to be activated in response to many kinds of brain damage and injury. Two recent studies employed *in vivo* TPLSM to directly visualize dynamic changes in microglia cell morphology in the neocortex of CX3CR1/EGFP mice (Davalos *et al.*, 2005; Nimmerjahn *et al.*, 2005). In both studies, time-lapse imaging was performed by repeatedly collecting small image stacks of EGFP-expressing microglial cells over the time course of several minutes to hours. Structural changes were analyzed from movies of the maximum-intensity projections. Surprisingly, microglial cells displayed an extraordinary level of restructuring even in their resting state. In contrast to neurons and astrocytes, which in the adult brain are mostly stable structures on the time scale of days and longer, microglial cells continually expand and retract their processes to interact with as well as screen the surrounding tissue components (Fig. 10.8A). The mean rate of length changes is about 1.5 μm/min (Fig. 10.8B). To get a sense of this rate, consider that the human cortex roughly contains 5×10^9 microglial cells, each possessing at least seven dynamic branches; thus the total restructuring of microglial cell processes in the human brain sums to 80,000 km/day.

Microglial cells are in a position to rapidly react to brain injury. For example, if focal lesions are produced by heating at a spot with the

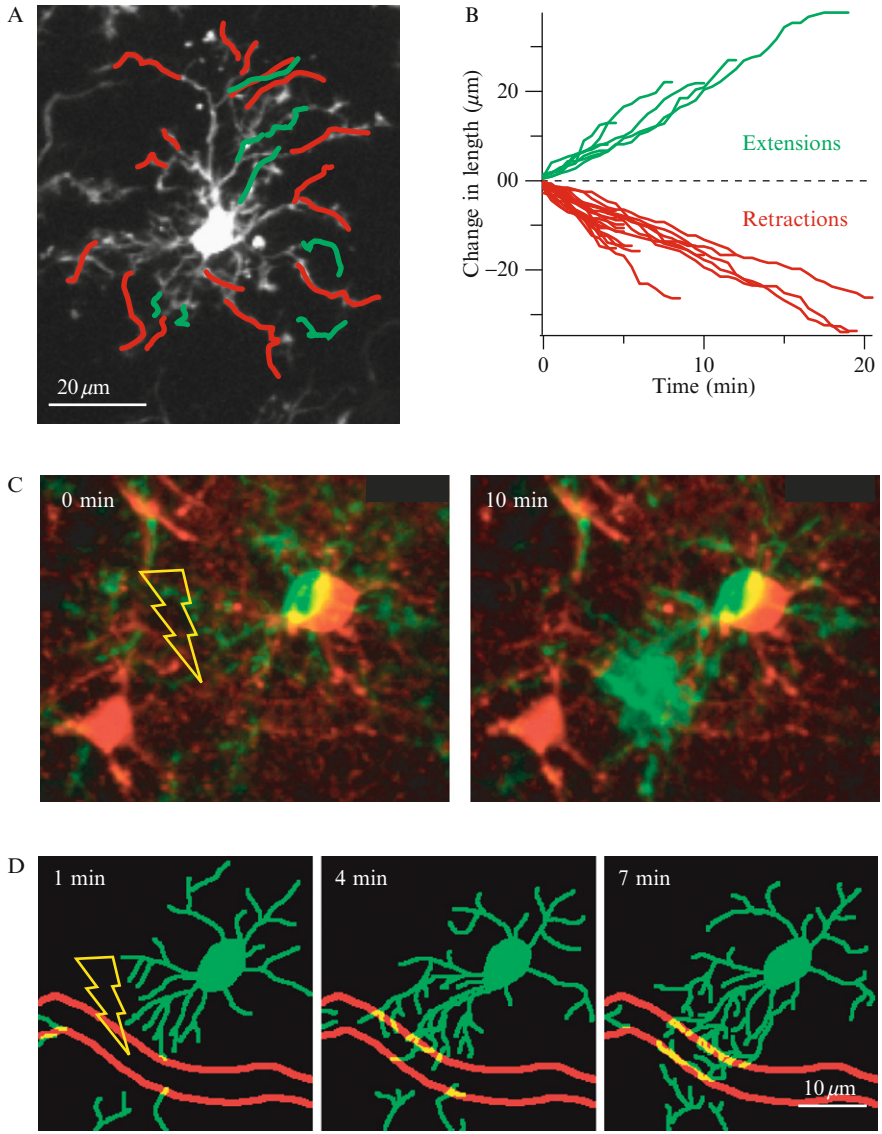

Figure 10.8 *In vivo* measurement of microglia function. (A) EGFP-expressing microglial cell in the neocortex of a CX3CR1/EGFP mouse. Extensions and retractions of cell processes over the time course of 20 min are indicated in green and red, respectively. (B) Length changes of the processes shown in (B) as a function of time. (C) Laser-induced damage to blood vessels causes a rapid focal response in neighboring microglial cells. Overlay of green microglia and SR101-stained astrocytes before and 10 min after a mild laser injury to a blood vessel. (D) Microglia morphology at intermediate time points during this event showing rapid, targeted movement of microglial processes toward the injured blood vessel (outlined in red); yellow flash indicates the site of injury. (Adapted from Nimmerjahn, A., Kirchhoff, F., and Helmchen, F. (2005). Resting microglial cells are highly dynamic surveillants of brain parenchyma *in vivo*. *Science* **308**, 1314–1318.)

same pulsed laser used for TPLSM, microglial processes are attracted by the injury site, switching their seemingly random patrolling behavior to a targeted response (Fig. 10.8C and D). The molecular mechanism underlying this structural activity involves extracellular ATP signaling (Davalos *et al.*, 2005; Haynes *et al.*, 2006). In the case of severe laser-induced disruptions of blood vessels, microglial cells become progressively activated over hours, exhibiting clear signs of phagocytosis (Nimmerjahn *et al.*, 2005). Quantification of microglia dynamics in the intact brain thus opens new opportunities for revealing molecular mechanisms of microglia activation and for studying their role in a variety of brain pathologies, such as Alzheimer's disease, multiple sclerosis, and ischemia.

3. Photoprocesses for Targeted Disruption of Vascular Flow

The ability to form occlusions in targeted pial arterioles and subsurface microvessels is an essential element in the study of microstrokes. A central question is how blockages in single small blood vessels lead to potential degradation of neuronal viability and the onset of tissue inflammation and necrosis.

3.1. Photoinduced thrombosis

The methods for targeted clot formation fall into two classes. The first makes use of the introduction of a photosensitizer into the blood stream and the subsequent irradiation of the target vessel with actinic light. This will drive photothrombosis and, with judicious adjustment of the intensity, will lead to a localized, focal blockage in surface vessels. This method is not appropriate for subsurface vessels, as clots will form along the entire path of the incident light-cone. Nonetheless, application of this technique led to an understanding of the redundancy in the pial arteriole network (Schaffer *et al.*, 2006) as well as to the identification of penetrating arterioles as the weak-link in the supply of blood from the pial vessels to the subsurface microvasculature (Nishimura *et al.*, 2007).

3.2. Plasma-mediated ablation

The ability to create an occlusion below the pial surface may be achieved solely with light through the use of plasma-mediated photoprocesses. This technique makes use of the dissociation of matter by high-fluence, ultrafast pulses of near-infrared laser light (~100 fs pulse duration). The pulse initially leads to ionization of the material, such as blood plasma or vascular

lumen, within a femtoliter-sized focal volume of the incident laser pulse. The interaction photogenerated free electrons and light toward the end of the laser pulse results in a spatially limited release of mechanical energy in the form of a shock wave (Joglekar *et al.*, 2004; Schaffer *et al.*, 2002). In practice, this method allows occlusions to be formed at least down to 500 μm below the pia without disruption of neighboring tissue.

The hardware for plasma-mediated occlusion is readily combined with TPLSM through a thinned skull window to enable the targeting and real-time monitoring of blood vessels. The typical set-up makes use of a standard two-photon microscope in which an additional amplified 100 fs light source is introduced to the beam path through a polarizing beam splitter (Fig. 10.9A). The imaging and photodisruption beams are brought to the same focus so that photodisruption occurs at the center of the imaged field. The energy per pulse of the amplified beam needs to be at least 0.03 μJ at the focus, which corresponds to a near-threshold fluence for damage of approximately 1 J/cm^2 with a 40× dipping objective. Calibration curves are established for each sample. The end result is the occlusion of flow in a targeted microvessel (Fig. 10.9B) (Nishimura *et al.*, 2006).

As an application, we consider a microvessel that lay approximately 250 μm below the pia (Fig. 10.9C). Uniform flow is seen in the vessel prior to irradiation, as evidenced by streaks in the raster-scanned imaged (panel 1 in Fig. 10.9C). After the first burst of amplified laser pulses, there was temporary cessation of RBC motion and swelling of the target vessel (panels 2 and 3 in Fig. 10.9C). Labeling of the vessel wall with trapped fluorescein/dextran is also observed, and flow rapidly returns (panels 2 and 3 in Fig. 10.9C). A second burst of pulses led to limited extravasation and permanent occlusion of the vessel lumen (panel 4 in Fig. 10.9C). Quantitative measurements of the speed and direction of RBC flow before and after formation of the occlusion (Fig. 10.6) indicate that blockage of flow in the microvessel further leads to the cessation of flow in vessels that lie immediately downstream of the occlusion (Fig. 10.9C).

4. Outlook

The technology for measuring blood flow at the level of individual vessels throughout the upper layers of neocortex (Kleinfeld *et al.*, 1998; Nishimura *et al.*, 2007; Schaffer *et al.*, 2006; Zhang and Murphy, 2007; Zhang *et al.*, 2005) and the olfactory bulb (Chaigneau *et al.*, 2003) is largely mature. Open issues on flow per se exist in three areas. The first concerns the absence of a map, or "plumbing diagram," of the connectivity of brain vasculature. Such a map is critical as a means to calculate potential modularity in the vascular system and correlations in flow, as well as the

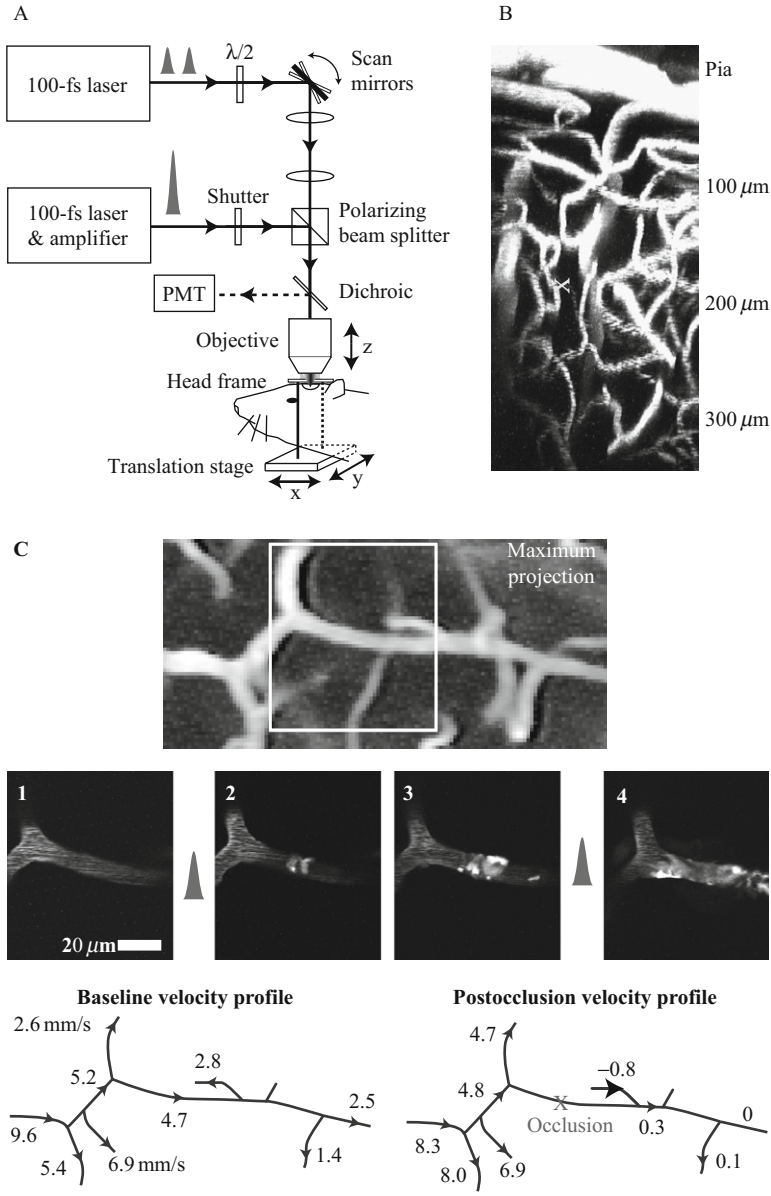

Figure 10.9 Formation of intravascular occlusions in deep microvessels using amplified 100-fs laser pulses. (A) Rough schematic of a TPLSM system modified for delivery of amplified 100-fs pulses. The polarizing beam splitter combined imaging and ablation beams. (B) An xz-projection of a TPLSM image stack that shows deep microvessels (yellow cross) that are routinely targeted for selective occlusion using this technique. (C) Maximum-intensity projection of a TPLSM stack showing a tortuous network of subsurface microvessels. The second row shows planar images taken from a region of

control of flow by neuronal and astrocytic activity. Preliminary anatomical work in this direction is promising (Tsai *et al.*, 2003; Weber *et al.*, 2008). The second issue is the need to measure both resilience and control of flow in subcortical areas, in particular the striatum, where vascularization is relatively sparse and damage from stroke relatively high compared with neocortex (Feekes and Cassell, 2006). Surgical resection and the use of small-diameter, gradient-index lenses for endoscopic imaging may enable such studies (Jung *et al.*, 2004; Levene *et al.*, 2004). The third issue in flow concerns the need to directly measure pressure, which at this time is only inferred and depends on estimates of "effective viscosity." A direct method would enable observation of homeostatic control at the level of microvessels. A viable approach for building an optical-based pressure sensor is unclear, but may involve reporters of the deformation of endothelial cells that comprise vessel walls.

The ability to observe calcium dynamics in astrocytes concomitant with changes in blood flow provides a means to study how astrocytes mediate the coupling of neuronal activity to changes in blood flow (Mulligan and MacVicar, 2004; Takano *et al.*, 2006). A second means of neuronal control involves direct control of vascular dilation or contraction by inhibitory interneurons (Cauli *et al.*, 2004). The advent of functional labeling of subpopulations of inhibitory cells will allow this critical but largely unexplored pathway to be studied *in vivo*. Of particular relevance for future work are the new Brainbow mice, in which glial cells as well as neuronal cell types are made to express FPs of different color in a combinatorial manner, resulting, for example, in a multicolor stain of the astrocytic network (Livet *et al.*, 2007). Moreover, glia-specific expression of genetically encoded FP-based calcium indicators (Garaschuk *et al.*, 2006b; Kotlikoff, 2007; Miyawaki, 2005) may foster new studies of glial function in the intact brain.

Experimental models of stroke are also poised to gain from measurements of functional changes in neurons and glial cells concomitant to those of changes of blood flow in response to targeted occlusion of vessels. The work of Murphy and colleagues explored the use of transgenic animals with GFP-labeled dendrites as a means to look at cellular changes that track

interest (white rectangle) depicting the time-course for intravascular clot formation (frames 1 to 4) in a specific, 10-μm-diameter vessel. The red pulses indicate irradiation with multiple trains of 0.03-μJ pulses delivered at 1 kHz. The third row shows vascular traces with baseline and postocclusion RBC velocity profiles, in millimeters per second, of the vascular network. Arrowheads denote the direction of RBC movement and the red cross marks the occluded microvessel. (Adapted from Nishimura, N., Schaffer, C. B., Friedman, B., Tsai, P. S., Lyden, P. D., and Kleinfeld, D. (2006). Targeted insult to individual subsurface cortical blood vessels using ultrashort laser pulses: Three models of stroke. *Nat. Methods* 3, 99–108.)

ischemia (Zhang *et al.*, 2005). Future work will likely involve chronic studies of changes in flow concomitant with changes in cell function. The latter may be measured with endogenous indicators of function, such as FP-based calcium indicators (Garaschuk *et al.*, 2007). Further, stroke-based research will benefit from real-time monitoring of microglia dynamics and direct visualization of invading immune effector cells, along with molecular components of clot formation (Ogawa *et al.*, 1990), such as platelets, fibrin, and thrombin, during ischemia.

A final point is that all measurements to date on blood flow, their control by neuronal and glial activity, and changes in molecular markers of tissue viability, have involved anesthetized animals. While anesthesia does not necessarily block homeostasis, it does affect the extent of modulation of the pial and deep brain vasculature by small neuroactive molecules such as acetylcholine. It is thus important to move towards recording in awake animals (Dombeck *et al.*, 2007). This is particularly important for the case of experimental stroke, where homeostasis may be compromised by anesthesia.

ACKNOWLEDGMENTS

Recent work in the Helmchen laboratory was funded by the Max Planck Society, the University of Zurich, and grants from the Human Frontier Science Program and the Swiss National Science Foundation. Recent work in the Kleinfeld laboratory was funded by grants from the National Science Foundation (Division of Biological Infrastructure) and the National Institutes of Health, National Center for Research Resources (NCRR), National Institute of Neurological Disorders and Stroke (NINDS), National Institute of Biomedical Imaging and Bioengineering (NIBIB). We thank Philbert Tsai and Pablo Blinder for supplying the unpublished data for Fig. 10.2, and Andy Shih for performing the analysis shown in Fig. 10.6D.

REFERENCES

Abbott, N. J., Rönnbäck, L., and Hansson, E. (2006). Astrocyte–endothelial interactions at the blood–brain barrier. *Nat. Rev. Neurosci.* **7,** 41–53.

Bacskai, B. J., Klunk, W. E., Mathis, C. A., and Hyman, B. T. (2002). Imaging amyloid-beta deposits *in vivo*. *J. Cerebral Blood Flow Metab.* **22,** 1035–1041.

Bacskai, B. J., Kajdasz, S. T., Christie, R. H., Carter, C., Games, D., Seubert, P., Schenk, D., and Hyman, B. T. (2001). Imaging of amyloid-beta deposits in brains of living mice permits direct observation of clearance of plaques with immunotherapy. *Nat. Med.* **7,** 369–372.

Brozici, M., van der Zwain, A., and Hillen, B. (2003). Anatomy and functionality of leptomeningeal anastomoses: A review. *Stroke* **34,** 2750–2762.

Cauli, B., Tong, X. K., Rancillac, A., Serluca, N., Lambolez, B., Rossier, J., and Hamel, E. (2004). Cortical GABA interneurons in neurovascular coupling: Relays for subcortical vasoactive pathways. *J. Neurosci.* **24,** 8940–8949.

Chaigneau, E., Oheim, M., Audinat, E., and Charpak, S. (2003). Two-photon imaging of capillary blood flow in olfactory bulb glomeruli. *Proc. Natl. Acad. Sci. U.S.A.* **100,** 13081–13086.

Cook, D. N., Chen, S. C., Sullivan, L. M., Manfra, D. J., Wiekowski, M. T., Prosser, D. M., Vassileva, G., and Lira, S. A. (2001). Generation and analysis of mice lacking the chemokine fractalkine. *Mol. Cell Biol.* **21,** 3159–3165.

Davalos, D., Grutzendler, J., Yang, G., Kim, J. V., Zuo, Y., Jung, S., Littman, D. R., Dustin, M. L., and Gan, W. B. (2005). ATP mediates rapid microglial response to local brain injury *in vivo*. *Nat. Neurosci.* **8,** 752–758.

Denk, W., Strickler, J. H., and Webb, W. W. (1990). Two-photon laser scanning fluorescence microscopy. *Science* **248,** 73–76.

Denk, W., Delaney, K. R., Kleinfeld, D., Strowbridge, B., Tank, D. W., and Yuste, R. (1994). Anatomical and functional imaging of neurons and circuits using two photon laser scanning microscopy. *J. Neurosci. Methods* **54,** 151–162.

Dombeck, D. A., Khabbaz, A. N., Collman, F., Adelman, T. L., and Tank, D. W. (2007). Imaging large-scale neural activity with cellular resolution in awake, mobile mice. *Neuron* **56,** 43–57.

Ehinger, B., Zucker, C. L., Bruun, A., and Adolph, A. (1994). *In vivo* staining of oligodendroglia in the rabbit retina. *Glia* **10,** 40–48.

Eichhoff, G., Busche, M. A., and Garaschuk, O. (2008). *In vivo* calcium imaging of the aging and diseased brain. *Eur. J. Nucl. Res. Mol. Med.* **35** (Suppl. 1), S99–S106.

Feekes, J. A., and Cassell, M. D. (2006). The vascular supply of the functional compartments of the human striatum. *Brain* **129,** 2189–2201.

Feng, G., Mellor, R. H., Bernstein, M., Keller-Peck, C., Nguyen, Q. T., Wallace, M., Nerbonne, J. M., Lichtman, J. W., and Sanes, J. R. (2000). Imaging neuronal subsets in transgenic mice expressing multiple spectral variants of GFP. *Neuron* **28,** 41–51.

Frostig, R. D., Dory, Y., Kwon, M. C., and Masino, S. A. (1993). Characterization of functional organization within rat barrel cortex using intrinsic signal optical imaging through a thinned skull. *Proc. Natl. Acad. Sci. U.S.A.* **90,** 9998–10002.

Fuss, B., Mallon, B., Phan, T., Ohlemeyer, C., Kirchhoff, F., Nishiyama, A., and Macklin, W. B. (2000). Purification and analysis of *in vivo*-differentiated oligodendrocytes expressing the green fluorescent protein. *Dev. Biol.* **218,** 259–274.

Garaschuk, O., Milos, R. I., and Konnerth, A. (2006a). Targeted bulk-loading of fluorescent indicators for two-photon brain imaging *in vivo*. *Nat. Protoc.* **1,** 380–386.

Garaschuk, O., Milos, R. I., Grienberger, C., Marandi, N., Adelsberger, H., and Konnerth, A. (2006b). Optical monitoring of brain function *in vivo*: From neurons to networks. *Pflugers Arch.* **453,** 385–396.

Garaschuk, O., Griesbeck, O., and Konnerth, A. (2007). Troponin C-based biosensors: A new family of genetically encoded indicators for *in vivo* calcium imaging in the nervous system. *Cell Calcium* **42,** 351–361.

Göbel, W., and Helmchen, F. (2007). *In vivo* calcium imaging of neural network function. *Physiology (Bethesda)* **22,** 358–365.

Grutzendler, J., Kasthuri, N., and Gan, W. B. (2002). Long-term dendritic spine stability in the adult cortex. *Nature* **420,** 812–816.

Haynes, S. E., Hollopeter, G., Yang, G., Kurpius, D., Dailey, M. E., Gan, W. B., and Julius, D. (2006). The P2Y(12) receptor regulates microglial activation by extracellular nucleotides. *Nat. Neurosci.* **9,** 1512–1519.

Helmchen, F., and Denk, W. (2002). New developments in multiphoton microscopy. *Curr. Opin. Neurobiol.* **12,** 593–601.

Helmchen, F., and Denk, W. (2005). Deep tissue two-photon microscopy. *Nat. Methods* **2,** 932–940.

Hirase, H., Qian, L., Bartho, P., and Buzsaki, G. (2004). Calcium dynamics of cortical astrocytic networks *in vivo*. *PLoS Biol*. **2,** e96.

Joglekar, A. P., Liu, H. H., Meyhofer, E., Mourou, G., and Hunt, A. J. (2004). Optics at critical intensity: Applications to nanomorphing. *Proc. Natl. Acad. Sci. U.S.A.* **101,** 5856–5861.

Jung, J. C., Mehta, A. D., Aksay, E., Stepnoski, R., and Schnitzer, M. J. (2004). *In vivo* mammalian brain imaging using one- and two-photon fluorescence microendoscopy. *J. Neurophysiol.* **92,** 3121–3133.

Jung, S., Aliberti, J., Graemmel, P., Sunshine, M. J., Kreutzberg, G. W., Sher, A., and Littman, D. R. (2000). Analysis of fractalkine receptor CX(3)CR1 function by targeted deletion and green fluorescent protein reporter gene insertion. *Mol. Cell Biol.* **20,** 4106–4114.

Kafitz, K. W., Meier, S. D., Stephan, J., and Rose, C. R. (2008). Developmental profile and properties of sulforhodamine 101-labeled glial cells in acute brain slices of rat hippocampus. *J. Neurosci. Methods*. **169,** 84–92.

Keifer, J., Vyas, D., and Houk, J. C. (1992). Sulforhodamine labeling of neural circuits engaged in motor pattern generation in the *in vitro* turtle brainstem-cerebellum. *J. Neurosci.* **12,** 3187–3199.

Kleinfeld, D., and Delaney, K. R. (1996). Distributed representation of vibrissa movement in the upper layers of somatosensory cortex revealed with voltage sensitive dyes. *J. Comp. Neurol.* **375,** 89–108.

Kleinfeld, D., and Griesbeck, O. (2005). From art to engineering? The rise of *in vivo* mammalian electrophysiology via genetically targeted labeling and nonlinear imaging. *Public Library Sci. Biol.* **3,** 1685–1689.

Kleinfeld, D., Mitra, P. P., Helmchen, F., and Denk, W. (1998). Fluctuations and stimulus-induced changes in blood flow observed in individual capillaries in layers 2 through 4 of rat neocortex. *Proc. Natl. Acad. Sci. U.S.A.* **95,** 15741–15746.

Kleinfeld, D., Friedman, B., Lyden, P. D., and Shih, A. Y. (2008). Targeted occlusion to surface and deep vessels in neocortex via linear and nonlinear optical absorption. *In* "Animal Models of Acute Neurological Injuries." (J. Chen, X.-M. Xu, and J. Zhang, eds.). Totowa: The Humana Press Inc.

Kotlikoff, M. I. (2007). Genetically encoded Ca^{2+} indicators: Using genetics and molecular design to understand complex physiology. *J. Physiol.* **578,** 55–67.

Levene, M. J., Dombeck, D. A., Kasischke, K. A., Molloy, R. P., and Webb, W. W. (2004). *In vivo* multiphoton microscopy of deep brain tissue. *J. Neurophysiol.* **91,** 1908–1912.

Livet, J., Weissman, T. A., Kang, H., Draft, R. W., Lu, J., Bennis, R. A., Sanes, J. R., and Lichtman, J. W. (2007). Transgenic strategies for combinatorial expression of fluorescent proteins in the nervous system. *Nat. Neurosci.* **450,** 56–62.

Miyawaki, A. (2005). Innovations in the imaging of brain functions using fluorescent proteins. *Neuron* **48,** 189–199.

Mulligan, S. J., and MacVicar, B. A. (2004). Calcium transients in astrocyte endfeet cause cerebrovascular constrictions. *Nature* **431,** 195–199.

Nimmerjahn, A., Kirchhoff, F., Kerr, J. N., and Helmchen, F. (2004). Sulforhodamine 101 as a specific marker of astroglia in the neocortex *in vivo*. *Nat. Methods* **29,** 31–37.

Nimmerjahn, A., Kirchhoff, F., and Helmchen, F. (2005). Resting microglial cells are highly dynamic surveillants of brain parenchyma *in vivo*. *Science* **308,** 1314–1318.

Nishimura, B., Schaffer, C. B., Friedman, B., Lyden, P. D., and Kleinfeld, D. (2007). Penetrating arterioles are a bottleneck in the perfusion of neocortex. *Proc. Natl. Acad. Sci. U.S.A.* **104,** 365–370.

Nishimura, N., Schaffer, C. B., Friedman, B., Tsai, P. S., Lyden, P. D., and Kleinfeld, D. (2006). Targeted insult to individual subsurface cortical blood vessels using ultrashort laser pulses: Three models of stroke. *Nat. Methods* **3,** 99–108.

Nolte, C., Matyash, M., Pivneva, T., Schipke, C. G., Ohlemeyer, C., Hanisch, U. K., Kirchhoff, F., and Kettenmann, H. (2001). GFAP promoter-controlled EGFP-expressing transgenic mice: A tool to visualize astrocytes and astrogliosis in living brain tissue. *Glia* **33,** 72–86.

Ogawa, S., Lee, T. M., Kay, A. R., and Tank, D. W. (1990). Brain magnetic resonance imaging with contrast dependent on blood oxygenation. *Proc. Natl. Acad. Sci. U.S.A.* **87,** 9868–9872.

Sarelius, I. H., and Duling, B. R. (1982). Direct measurement of microvessel hematocrit, red cell flux, velocity, and transit time. *Am. J. Physiol.* **243,** H1018–H1022.

Schaffer, C. B., Nishimura, N., Glezer, E. N., Kim, A. M. T., and Mazur, E. (2002). Dynamics of femtosecond laser-induced breakdown in water from femtoseconds to microseconds. *Opt. Express* **10,** 196–203.

Schaffer, C. B., Friedman, B., Nishimura, N., Schroeder, L. F., Tsai, P. S., Ebner, F. F., Lyden, P. D., and Kleinfeld, D. (2006). Two-photon imaging of cortical surface microvessels reveals a robust redistribution in blood flow after vascular occlusion. *Public Library Sci. Biol.* **4,** 258–270.

Stosiek, C., Garaschuk, O., Holthoff, K., and Konnerth, A. (2003). *In vivo* two-photon calcium imaging of neuronal networks. *Proc. Natl. Acad. Sci. U.S.A.* **100,** 7319–7324.

Takano, T., Tian, G. F., Peng, W., Lou, N., Libionka, W., Han, X., and Nedergaard, M. (2006). Astrocyte-mediated control of cerebral blood flow. *Nat. Neurosci.* **9,** 260–267.

Tian, G. F., Azmi, H. T. T., Xu, Q., Peng, W., Lin, J., Oberheim, N., Lou, N., Wang, X., Zielke, H. R., Kang, J., and Nedergaard, M. (2005). An astrocytic basis of epilepsy. *Nat. Med.* **11,** 973–981.

Tsai, P. S., Friedman, B., Schaffer, C. B., Squier, J. A., and Kleinfeld, D. (2005). All-optical, *in situ* histology of neuronal tissue with femtosecond laser pulses. *In* "Imaging in Neuroscience and Development: A Laboratory Manual." (R. Yuste and A. Konnerth, eds.), pp. 815–826. Cold Spring Harbor Laboratory Press, New York.

Tsai, P. S., Friedman, B., Ifarraguerri, A. I., Thompson, B. D., Lev-Ram, V., Schaffer, C. B., Xiong, Q., Tsien, R. Y., Squier, J. A., and Kleinfeld, D. (2003). All-optical histology using ultrashort laser pulses. *Neuron* **39,** 27–41.

Vermeer, S. E., Prins, N. D., den Heijer, T., Hofman, A., Koudstaal, P. J., and Breteler, M. M. (2003). Silent brain infarcts and the risk of dementia and cognitive decline. *N. Engl. J. Med.* **348,** 1215–1222.

Volterra, A., and Meldolesi, J. (2005). Astrocytes, from brain glue to communication elements: The revolution continues. *Nat. Rev. Neurosci.* **6,** 626–640.

Wang, X., Lou, N., Xu, Q., Tian, G. F., Peng, W. G., Han, X., Kang, J., Takano, T., and Nedergaard, M. (2006). Astrocytic Ca^{2+} signaling evoked by sensory stimulation *in vivo*. *Nat. Neurosci.* **9,** 816–823.

Weber, B., Keller, A. L., Reichold, J., and Logothetis, N. K. (2008). The microvascular system of the striate and extrastriate visual cortex of the macaque. *Cerebral Cortex* **18,** 2318–2330.

Zhang, S., and Murphy, T. H. (2007). Imaging the impact of cortical microcirculation on synaptic structure and sensory-evoked hemodynamic responses *in vivo*. *Public Library Sci. Biol.* **5,** e119.

Zhang, S., Boyd, J., Delaney, K. R., and Murphy, T. H. (2005). Rapid reversible changes in dendritic spine structure *in vivo* gated by the degree of ischemia. *J. Neurosci.* **25,** 5333–5228.

Zhuo, L., Sun, B., Zhang, C. L., Fine, A., Chiu, S. Y., and Messing, A. (1997). Live astrocytes visualized by green fluorescent protein in transgenic mice. *Dev. Biol.* **187,** 36–42.